Evolution of Kinetic and Magnetic Energy in Intra Cluster Media

Kiwan Park

Department of Physics, UNIST, Ulsan, 689798, Korea; pkiwan@unist.ac.kr

Dongho Park

APCPT, Pohang, 790784, Korea; dongho@apctp.org

ABSTRACT

Intra Cluster Media (ICMs) located at galaxy clusters is in the state of hot, tenuous, magnetized, and highly ionized X-ray emitting plasmas. This overall collisionless, viscous, and conductive magnetohydrodynamic (MHD) turbulence in ICM is simulated using hyper and physical magnetic diffusivity. The results show that fluctuating random plasma motion amplifies the magnetic field, which cascades toward the diffusivity scale passing through the viscous scale. The kinetic eddies in the subviscous scale are driven and constrained by the magnetic tension which finally gets balanced with the highly damping effect of the kinetic eddies. However, the saturated kinetic energy spectrum is deeper than that of the incompressible or compressible hydrodynamics fluid. To explain this unusual field profile we set up two simultaneous differential equations for the kinetic and magnetic energy spectrum using an Eddy Damped Quasi Normal Markovianized (EDQNM) approximation. The analytic solution tells us that the magnetic energy in addition to the viscous damping effect constrains the plasma motion leading to the power spectra: kinetic energy spectrum $E_V^k \sim k^{-3}$ and corresponding representative magnetic energy spectrum $E_M^k \sim k^{-1/2}$. Also the comparison of simulation results with different resolutions and magnetic diffusivities implies the role of small scale magnetic energy in dynamo.

Subject headings: galaxies: clusters: intracluster medium, magnetic fields

1. Introduction

ICM located at the center of galaxy cluster is composed of fully ionized hot plasmas ($T \sim 10^8$K). The gas includes most of the cluster baryons ($> 85\%$) and heavy elements, but overall density 'n' is very low ($n < 10^3\, cm^{-3}$). As a result ICM has very small diffusivity

'η' ($\sim T^{-3/2}$) while viscosity 'ν' ($\sim 1/n$) is very large (Schekochihin et al. 2005). Dynamo effect from the turbulent flow motions in ICM exceeds the dissipation of such high viscous plasmas causing the growth of seed magnetic fields, which react back the plasma motion through magnetic tension ($\mathbf{B}\cdot\nabla\mathbf{B}$).

The amplified magnetic field constrains some intrinsic properties in ICM. Non-magnetized thermal Spitzer conductivity 'κ_{SP}' is like (Narayan & Medvedev 2001):

$$\kappa_{SP} \sim \frac{\lambda_{\rm e}^2}{t_{coul}} \sim 4\times 10^{32} T_1^{5/2} n_{-3}^{-1}\,{\rm cm}^2\,s^{-1}, \tag{1}$$

where $T_1 = kT/10$ Kev, $\lambda_{\rm e}$ is the mean free path of an electron and t_{coul} is the time between coulomb collisions. If magnetic field is injected, $\kappa_\perp$, conductivity perpendicular to the magnetic field is reduced to $\sim (\rho_e/\lambda_e)^2\kappa_{SP} (\ll \kappa_{SP})$ so that the conductivity becomes anisotropic with one third of the thermal Spitzer conductivity: $\kappa = \kappa_\perp + \kappa_\parallel \rightarrow \kappa_\parallel$. This anisotropic conductivity brings about temperature distribution that depends on the direction and strength of magnetic field. Also as the conservation of magnetic moment $\mu_B = u_\perp^2/B$ and kinetic energy ($\sim u_\parallel^2 + u_\perp^2$) implies, magnetic field makes pressure tensor $P_{ij} = mn\overline{u_i u_j}$ anisotropic along the field. The ratio of pressure anisotropy '$\triangle$' is implicitly related to the viscosity and stability of ICM (Schekochihin et al. 2010):

$$\triangle \;\equiv\; \frac{p_\perp - p_\parallel}{p} \sim \frac{1}{\nu_{ii}}\frac{1}{B}\frac{dB}{dt} \in \left[-\frac{2}{\beta}, \frac{1}{\beta}\right], \qquad (\beta = 8\pi p/B^2). \tag{2}$$

Here, kinematic viscosity $\nu \sim u_{th}^2/\nu_{ii}$, ion-ion collision frequency $\nu_{ii} = 4\pi n e^4 \ln\Lambda\, m_i^{-1/2} T^{3/2}$. If $\triangle$ is smaller than $-2/\beta$ or larger than $1/\beta$, firehose or mirror instability occurs in the range between ion Larmor radius ($\rho_i \sim 10^4 - 10^6$ km) and the mean free path ($\lambda_{\rm mfp}\sim 10^{15}$ km) (Schekochihin et al. 2008). Since ICM has high 'β', stability range is very narrow, i.e., practically unstable. Instability is thought to redistribute the plasma motions faster than coulomb collision does, but its role is not fully understood yet (Jones 2008).

By now we may begin to wonder if a typical MHD theory is applicable to the weakly collisional ICM plasma. Since collision between particles transfers momentum to make the system isotropic, most phenomenological or analytic methods assume the collisional MHD system system. However, since the tenuous plasmas cannot expect sufficient collisions, Chew, Goldberger, and Low (Chew et al. 1956) developed an adiabatic MHD equation with the consideration of anisotropic pressure tensor (CGL-MHD model). Recently Santos-Liman insisted the validness of the typical MHD theory with these additional constraints (Santos-Lima et al. 2011, 2014). Their model, a kinetic MHD based on CGL-closure with the limit of anisotropy,

shows the growth rate of magnetic energy is similar to that of a typical MHD theory in the early time regime, but the saturation is much smaller. In fact, the effect of anisotropy due to the magnetic field in the plasma does not appear in the kinematic regime while magnetic back reaction is negligibly small.

However, regardless of the anisotropic limit, the fluids driven by a random and isotropic external force eventually become isotropic followed by the strongly frozen magnetic fields if $Pr_M \rightarrow \infty$ ($\eta \rightarrow 0$). Even for a unit magnetic prandtl number ($Pr_M = \nu/\eta = 1$), where magnetic fields are not so strongly frozen, the large scale fields driven by the random isotropic force tend to remain independent of direction if a background magnetic field '$\mathbf{b}_{ext}$' is not very strong (Cho et al. 2009). Moreover the growing anisotropy in smaller scales cannot decisively affect the energy spectrum due to the small eddy turnover time. As long as the isotropic force continuously drives the system, especially large scales, the theoretical fluid model that assumes an isotropic system is valid except the case of microscale instability or very strong '$\mathbf{b}_{ext}$'. In addition there is an interesting report that the magnetic energy spectrum around the core of cluster is possibly Kolmogorov's spectrum $\sim k^{-5/3}$ (Kolmogorov 1941) which assumes an isotropic system (Vogt & Enßlin 2003). Now we can focus our interest on the isotropic properties in ICM of large magnetic prandtl number: energy spectra.

Dynamo in magnetized plasma with large Pr_M, which is not rarely observed in space, occurs easily and has its peculiar properties. As the excited magnetic fields (energy) are instilled into the damped kinetic eddies, the viscous damping scale $k_\nu \sim 1/l_\nu$ is extended toward resistivity scale $k_\eta \sim 1/l_\eta$ ($k_\nu \ll k_\eta$). Then, these two coupled velocity and magnetic field generate specific power spectra which are different from the typical spectrum of Kolmogorov's incompressible fluid or Burger's compressible fluid. There have been works on the small scale dynamo for large Pr_M plasma (Schekochihin et al. 2002; Cho et al. 2003; Schekochihin et al. 2004; Yousef et al. 2007) in addition to the several analytic methods (Batchelor 1950; Kazantsev 1968; Kulsrud and Anderson 1992; Schober et al. 2012; Bovino et al 2013). To solve the magnetic induction equation MHD theories based on Kazantsev's work (Kazantsev 1968) assume the second order velocity field correlation $\langle \mathbf{v} \cdot \mathbf{v} \rangle \sim (\delta_{ij} - \frac{r_i r_j}{r^2}) T_N(r) + \frac{r_i r_j}{r^2} T_L(r)$. However to explain the formation of this second order velocity field correlation, i.e., kinetic energy spectrum, we need to solve the coupled momentum and magnetic induction equation simultaneously instead of making an assumption of the kinetic energy spectrum in advance. Here we use an Eddy Damped Quasi Normal Markovianization method EDQNM, (Kraichnan & Nagarajan 1967; McComb 1990; Park 2013) and dimensional approach in a limited way. We simplified the resultant simultaneous differential equations and found out the solutions for kinetic and magnetic energy spectrum.

In chapter 2, we briefly introduce simulation tool and analytic method used in this paper. Simulational and analytic results are introduced in chapter 3. And in the final chapter we discuss about the results, their physical meanings, and future topics. Detailed analytic calculations are discussed in the appendix.

2. Numerical and analytic method

We have solved the incompressible MHD equations using a pseudo-spectral code with a periodic box of size '$(2\pi)^3$':

$$\frac{\partial \mathbf{v}}{\partial t} = -\mathbf{v}\cdot\nabla\mathbf{v} - \nabla P + (\nabla\times\mathbf{B})\times\mathbf{B} + \nu\nabla^2\mathbf{v} + \mathbf{f}, \quad (3)$$

$$\frac{\partial \mathbf{B}}{\partial t} = \nabla\times(\mathbf{v}\times\mathbf{B}) + \mathbf{b}_{\rm ext}, \quad (4)$$

where '$\mathbf{f}$' is a random mechanical force driving a system at $k \sim 2-3$ in fourier space, and '$\mathbf{b}_{\rm ext}$' is a weak background (guide) magnetic field[1] ($b_{ext} = 0.0001$) covering the whole magnetic eddy scales. Here, '$\mathbf{B}$', magnetic field divided by '$(4\pi\rho)^{1/2}$', has the unit of Alfvén velocity, and '$\mathbf{v}$' is 'rms velocity', and 't' has the unit of large scale eddy turnover time 'L/v'. For example, if 'L' of a cluster is ~ 400 kpc and 'v' is ~ 400 km/s, then 'L/v' is $\sim 10^9$ year. The time 't' has the unit of '10^9' year. The system realizes the state of ICM of the high viscous plasma state with ideally frozen magnetic fields.

To compare the effect of hyper diffusivity (incompressible fluid) and physical diffusivity (compressible fluid), we also used PENCIL CODE (Brandenburg 2001) with message passing interface(MPI) in a periodic box of spatial volume $(2\pi)^3$ with mesh size 288^3. The basic equations solved in the code are,

$$\frac{D\rho}{Dt} = -\rho\nabla\cdot\mathbf{u} \quad (5)$$

$$\frac{D\mathbf{u}}{Dt} = -c_s^2\nabla\ln\rho + \frac{\mathbf{J}\times\mathbf{B}}{\rho} + \nu\big(\nabla^2\mathbf{u} + \frac{1}{3}\nabla\nabla\cdot\mathbf{u}\big) + \mathbf{f} \quad (6)$$

$$\frac{\partial \mathbf{A}}{\partial t} = \mathbf{u}\times\mathbf{B} - \eta\,\nabla\times\mathbf{B}. \quad (7)$$

[1] '$\mathbf{b}_{ext}$' is not indispensable for the growth of magnetic fields if there is a substituting seed magnetic field. The turbulence by cosmological shocks can amplify the weak seed field of any origin (Ryu et al. 2008). It was pointed out that subsonic turbulence could develop with a very weak seed magnetic field (Ryu et al. 2012). Moreover turbulence can amplify a localized seed magnetic field (Brandenburg 2001; Cho & Yoo 2012). Cho (Cho 2014) investigated the origin of seed magnetic fields and insisted that the origin of the seed field should be more like the localized seed magnetic fields ejected from the astrophysical bodies

ρ: density; $\mathbf{u}$: velocity; $\mathbf{B}$: magnetic field; $\mathbf{A}$: vector potential; $\mathbf{J}$: current density; $D/Dt(= \partial/\partial t + \mathbf{u}\cdot\nabla)$: advective derivative; η: magnetic diffusivity$(=c^2/4\pi\sigma$, σ: conductivity); ν: kinematic viscosity$(=\mu/\rho$, μ: viscosity); c_s: sound speed. Velocity is expressed in units of c_s, and magnetic fields in units of $(\rho_0\,\mu_0)^{1/2}c_s([B] = \sqrt{\rho_0\,[\mu_0]}[v]$ from $E_M \sim B^2/\mu_0$ and $E_{kin} \sim \rho_0 v^2)$. μ_0 is magnetic permeability and ρ_0 is the initial density. Note that $\rho_0 \sim \rho$ in the weakly compressible simulations. These constants c_s, μ_0, and ρ_0 are set to be '1'. $\mathbf{f}(x,t)$ is represented by $N\,\mathbf{f}_0(t)\,exp\,[i\,\mathbf{k}_f(t)\cdot\mathbf{x}+i\phi(t)]$($N$: normalization factor, $\mathbf{f}_0$: forcing magnitude, $\mathbf{k}_f(t)$: forcing wave number[2]. The variables are also independent of a unit system. However, instead of $\mathbf{b}_{ext}$, PENCIL CODE gives a system initial seed magnetic field in small scales. This seed field disappears in a few simulation time steps. PENCIL CODE and the other code (Cho et al. 2003) are not the same in various ways, but we will see they produce practically the same energy spectra.

3. Results

3.1. Simulation results

Fig.1(a) shows the normalized kinetic energy $E_V(t)$ (black dashed line) and magnetic energy $E_M(t)$ (red solid line) of incompressible MHD fluid ($\nu = 0.015$, $\eta \to 0$, $Pr_M \to \infty$, $\beta = 8\pi P/B^2 \to \infty$) with resolution of 256^3 (thinner line) and 512^3 (thicker line). Reynolds number Re of both cases are ~ 42, and their magnetic Reynolds number Re_M are actually infinity. When the random isotropic forcing begins to drive the system, $E_V(t)$ quickly grows, becomes saturated, and keeps the status quo until $E_M(t)$ begins to arise at $t \sim 15-20$. As $E_M(t)$ grows, the energy transfer from $E_V(t)$ to $E_M(t)$ gets accelerated. For this nonlocal energy transfer, the gap between kinetic and magnetic energy is an important factor. However, as $\mathbf{B}\cdot\nabla\mathbf{v}$ in Eq.(4) implies, the geometrical constraint between $\mathbf{v}$ and $\mathbf{B}$ also plays a role of determinant. If magnetic field is parallel to the gradient of velocity field, kinetic energy is transferred to magnetic eddies. If not, magnetic field frozen to the plasma fluid moves freely along the fluid or gets annihilated. Around the onset position at $t \sim 15-20$, structural change between E_V and E_M seems to get accelerated and completed at the saturation. Also the plot shows the onset position of $E_M(t)$ is proportional to the resolution. Higher resolution without resistivity makes more space where the forward cascaded $E_M(t)$ can stay not being dissipated much. This leads to the imbalanced energy distribution like the relatively smaller amount of magnetic energy in large scales and more amount of magnetic energy in

[2]Pencil code selects one of 350 vectors in k_f vector set at each time step. f_0 is 0.08 and injection scale $|k_f|$ is $\sim 1-2$

small scales. This makes the gap between E_V and E_M in large scales, especially around the injection scale, increase so that the nonlocal energy transfer become accelerated. The saturated magnetic energy $E_{M,sat}$ grows with the increase of resolution, but the saturated kinetic energy $E_{V,sat}$ decreases. This is the special feature of $\eta \sim 0$ with a fixed high viscosity.

Fig.1(b) includes the normalized $E_V(t)$ and $E_M(t)$ of compressible fluids. Their properties are as follows; for thicker line, Pr_M=75, $\nu = 0.015$, $\eta = 2\times10^{-4}$, $Re \sim 170$, $Re_M \sim 1.3\times10^4$, $\beta \sim 83$; for the thinner line, Pr_M=7500, $\nu = 0.015$, $\eta = 2\times10^{-6}$, $Re \sim 120$, $Re_M \sim 8.8\times10^5$, $\beta \sim 430$. The resolutions in both cases are 288^3. Since the average of Mach number is at most 0.18, the effect of compressibility is not much. We can infer more E_V can be transferred to E_M with higher Pr_M (lower η). However, the plot shows the actual $E_{V,sat}$ & $E_{M,sat}$ are inversely proportional to Pr_M. Moreover $E_{V,sat}$ is slightly larger than $E_{M,sat}$, and this tendency is opposite to that of hyper diffusivity (Fig.1(a)). If η is small, magnetic energy can migrate into the smaller scales. But since the effect of dissipation grows with the wave number k^2, more E_M is dissipated to increase energy gap between E_V and E_M. This boosts the nonlocal energy transfer bringing about the accelerated dissipation of energy ($\sim k^2E(k)$) in small scales. So the saturated energy $E_{V,sat}$, $E_{M,sat}$ are smaller than those of lower Pr_M. However, it is not easy to conclude whether they converge on some lower limit as the physical diffusivity $\eta \to 0$ with the limited resolution and Pr_M at this moment.

Fig.2(a) shows the evolving energy spectrum $E_V(k)$ and $E_M(k)$ of the incompressible fluid in the early time regime $t \sim 0 - 10.5$ (from bottom to top). And the plot in Fig.2(b) is a de facto the same one in the range of $t = 24.9 - 32.6$. When the kinetic energy begins to drive the system at $k = 2.5$, E_V (black dashed line, $t \sim 0$) grows prior to E_M (red solid line). As the advection term $\mathbf{v}\cdot\nabla\mathbf{v}$ indicates, E_M is not necessary for the local energy transfer in kinetic eddies. However, without $E_V(k)$ magnetic eddies cannot receive energy from kinetic eddies nor transfer its energy to the neighboring eddies. Only when magnetic fields run into the plasma fluids with the nontrivial E_V of which gradient is in the direction of magnetic fields, dynamo process occurs leading to the growth of E_M. Thus, in the very early time regime the evolution of magnetic field looks subsidiary. But around $t \sim 1.4 - 2.1$ $E_M(k)$ in small scales begins to surpass $E_V(k)$, and gets past $E_V(k)$ which suffers from the viscous dissipation. So most of E_V is located near the injection scale where the viscous damping effect is not so much, but E_M cascades forward and stays in the smaller scales. Kinetic eddies in $k <\sim 15$ lose energy (or magnetic eddies receive energy through $\mathbf{B}\cdot\nabla\mathbf{v}$) whereas smaller scale kinetic eddies ($k >\sim 15$) receive energy through magnetic tension $\mathbf{B}\cdot\nabla\mathbf{B}$. As the fluid motion can amplify the magnetic field through dynamo process, also magnetic fields can increase the kinetic energy through Lorentz force ($\mathbf{J}\times\mathbf{B}$). The magnetic fields press the

fluid through magnetic pressure ($-\nabla B^2/2$) and stretch the fluid through magnetic tension. We will see that the unusual $E_V(k)$ spectrum k^{-3} is due to not only the viscous damping but also the interaction with E_M.

Fig.3(a), 3(b) include the saturated energy spectra of incompressible fluids with hyper diffusivity. Also the saturated energy spectra of compressible fluids with physical diffusivity are shown in Fig.3(c), 3(d). These plots show $E_{V,sat}(k)$ eventually converges to $\sim k^{-3}$ if Pr_M is not too small regardless of the different evolving profiles of $E_V(t)$ and $E_M(t)$ in Fig.1(a), 1(b). So the comparison of these plots will give us some clues to the formation of $E_V(k)$ in small scale range. A quick look shows $E_V(k)$ of 512^3 has clear spectrum of k^{-3} compared with the kinetic energy spectrum of 256^3. However, these two simulation sets have the same conditions: weak $\mathbf{b}_{ext} = 0.0001$, isotropic random driving force $\mathbf{f}$, injection scale $k_f \sim 2.5$, viscosity $\nu = 0.015$, and negligible magnetic diffusivity η. Also the saturated energy levels shown in Fig.1(a) are not much different. Just the distribution of E_M of 512^3 in small scale is flatter than that of 256^3. This implies E_M in smaller scales may be a determinant of E_V spectrum.

On the other hand, for the compressible system in Fig.3(c) and Fig.3(d), $E_V(k)$ of $Pr_M = 7500$ has clearer and longer spectrum of k^{-3} despite its smaller saturated energy level: $E(t)_{sat.,\,Pr_M=75} > E(t)_{sat.,\,Pr_M=7500}$(Fig.1(b)). This means $E_{V,sat.}(k)$ is not so much influenced by the magnitude of $E_M(k)$. However, careful look shows the peak of E_M in Fig.3(d) is located at smaller scale regime than that of Fig.3(c). Then kinetic eddies in wider range can interact with magnetic energy $E_M(k)$ whose power spectrum is less steep. In other words, Fig.3(b) and Fig.3(d) commonly show the slope of $E_M(k)$ is not so slanted as that of Fig.3(a) and Fig.3(c).

So if we assume a critical representative spectrum $E_M(k) \sim k^m$ in the subviscous regime, we can infer that steeper spectrum than k^m cannot provide the kinetic eddies with enough energy for $E_V \sim k^{-3}$. However the exact value of 'm' is not known yet. Just we can guess this index should be negative. The scaling factor 'k^{-1}', so called an invariant scaling factor (Ruzmaikin et al. 1982; Kleeorin et al. 1996), is drawn together in next figure for reference. But we will not discuss this concept further in this paper.

Fig.4(a), 4(b) include the compensated k^3E_V and $k^{1/2}E_M$. $E_V(k)$ of high Pr_M has clear spectrum of k^{-3} in the subviscous scale. But for the spectrum of E_M in Fig.4(b), it is ambiguous to pinpoint any scaling factor. Instead, we choose '$k^{-1/2}$', i.e., $m = -1/2$, an

approximate median value of the previous results (Cho et al. 2003; Lazarian et al. 2004; Schekochihin et al. 2004). We will see analytic method derives quite exact $E_V(k)$ with this scaling factor $k^{-1/2}$. A reference line 'k^{-1}' for the scaling invariant factor is drawn together.

Fig.5(a) shows E_M/E_V for fig.3(a)-3(d). The ratio of hyper diffusivity is larger than that of physical diffusivity, which is consistent. As mentioned, with the negligible diffusivity the ratio proportionally depends on the resolution because of the larger E_M. In contrast, for the case of physical diffusivity (black line), the dissipation effect growing with wave number ($\sim k^2$) dissipates E_M more efficiently until the energy states are balanced to be in the state of equipartition.

3.2. Analytic methods & results

3.2.1. Eddy Damped Quasi Normal Markovianization

We start from the momentum (Eq.3) and magnetic induction equation (Eq.4). Taking divergence of the momentum equation we can replace pressure by convection and magnetic tension (Leslie and Leith 1975, Yoshizawa 2011)[3]:

$$\frac{\partial v_i(k,t)}{\partial t} = \sum_{p+r=k} M_{iqm}(k)[v_q(p,t)v_m(r,t) - B_q(p,t)B_m(r,t)] + \nu\nabla^2 v_i(k,t), \tag{8}$$

$$\frac{\partial B_i(k,t)}{\partial t} = \sum_{p+r=k} M^B_{iqm}(k)v_q(p,t)B_m(r,t), \tag{9}$$

with the definition of algebraic multipliers

$$\begin{aligned} M_{iqm}(k) &= -\frac{i}{2}\big(k_m\delta_{iq} + k_q\delta_{im} - \frac{2k_ik_qk_m}{k^2}\big), \\ M^B_{iqm}(k) &= i(k_m\delta_{iq} - k_q\delta_{im}). \end{aligned} \tag{10}$$

[3]'$v(k,t)$' and '$B(k,t)$' depend on time 't' and wavenumber 'k', but 't' will be omitted for simplicity.

Then we can get the evolving second order correlation equations of $\langle v_i(k)v_i(-k)\rangle$ and $\langle B_i(k)B_i(-k)\rangle$:

$$\big(\frac{\partial}{\partial t}+2\nu k^2\big)\langle v_i(k)v_i(-k)\rangle = \sum_{p+r=k} M_{iqm}(k)[\overbrace{\langle v_q(p)v_m(r)v_i(-k)\rangle}^{A1} - \overbrace{\langle v_q(-p)v_m(-r)v_i(k)\rangle}^{A2} - \overbrace{\langle B_q(p)B_m(r)v_i(-k)\rangle}^{A3} + \overbrace{\langle B_q(-p)B_m(-r)v_i(+k)\rangle}^{A4}], \quad (11)$$

$$\frac{\partial}{\partial t}\langle B_i(k)B_i(-k)\rangle = \sum_{p+r=k} M^B_{iqm}(k)[\overbrace{\langle v_q(p)B_m(r)B_i(-k)\rangle}^{B1} - \overbrace{\langle v_q(-p)B_m(-r)B_i(k)\rangle}^{B2}]. \quad (12)$$

The third order correlation, '$A1, A2, ..., B2$', is called a transport function. These triple correlations play a role of transfer and dissipation of energy to decide the field profiles of the system. If the field is helical, 'α' coefficient ($\sim \langle \mathbf{j}\cdot\mathbf{b}\rangle - \langle \mathbf{v}\cdot\omega\rangle$) for the inverse cascade of magnetic energy can be derived. Also other terms for the forward cascade of energies are derived (Krause & Rädler 1980; Moffatt 1978; Park & Blackman 2012a,b; Pouquet et al. 1976). However the helical field is not assumed in our system, which means 'α' coefficient or the inverse cascade of magnetic energy is excluded. We use a quasi normalization approximation, sort of an iterative method, to find the transport function (appendix).

The formal representations of $E_V(k)$ and $E_M(k)$ are as follows:

$$\begin{aligned}\frac{\partial E_V(k)}{\partial t} &= +\frac{1}{2}\int dp\,dr\,\Theta^{\nu\nu\nu}_{kpr}(t)\frac{k^3}{p\,r}(1-2y^2z^2-xyz)E_V(p)E_V(r)\\ &\quad -\int dp\,dr\,\Theta^{\nu\nu\nu}_{kpr}(t)\frac{p^2}{r}(xy+z^3)E_V(r)E_V(k)-2\nu k^2E_V(k)\\ &\quad +\frac{1}{2}\int dp\,dr\,\Theta^{\nu\eta\eta}_{kpr}(t)\frac{k^3}{p\,r}(1-2y^2z^2-xyz)E_M(p)E_M(r)\\ &\quad +\int dp\,dr\,\Theta^{\nu\eta\eta}_{kpr}(t)\frac{p^2}{r}(y^2z-z)E_M(r)E_V(k),\end{aligned} \quad (13)$$

and

$$\begin{aligned}\frac{\partial E_M(k)}{\partial t} &= -\int dp\,dr\,\Theta^{\eta\eta\nu}_{krp}(t)\frac{p^2}{r}z(1-x^2)E_M(r)E_M(k)\\ &\quad -\int dp\,dr\,\Theta^{\eta\eta\nu}_{krp}(t)\frac{r^2}{p}(y+xz)E_V(p)E_M(k)\\ &\quad +\int dp\,dr\,\Theta^{\eta\eta\nu}_{krp}(t)\frac{k^3}{p\,r}(1+xyz)E_V(p)E_M(r).\end{aligned} \quad (14)$$

The integral variables 'p', 'r', i.e., wavenumbers, are constrained by the relation of $p+r=k$. 'x', 'y', and 'z' are cosines of the angles formed by three vectors '**k**', '**p**', and '**r**'. (Fig.5(a)). Algebraically 'k', 'p', and 'r' should satisfy a condition like (Leslie and Leith 1975):

$$|k-r| \leq p \leq k+r. \tag{15}$$

To derive analytically solvable equations from Eq.(13), (14), we need to simplify these two equations considering the interaction between 'k' and its close wave number. So, we take account of only two cases: large p ($k \sim p \gg r$) and large r ($k \sim r \gg p$). In principle '$k/2 \sim p \sim r$' should also be included. But since the interaction between the close wave vectors, local energy transfer, is dominant in the nonhelical small scale dynamo, the latter case can be ignored.

With the assumption of $E_V(k) \sim k^v$ and $E_M(k) \sim k^m$, we simplify the first term in Eq.(14) like below:
(i) Large p (small r, i.e., $k \sim p \gg r$, $\eta \sim 0$)
Eddy damping function $\Theta^{\eta\eta\nu}_{krp}(k,t)$ is approximately

$$\Theta^{\eta\eta\nu}_{krp}(k,t) = \left.\frac{1-e^{-[\nu p^2+\eta(k^2+r^2)+\mu_{kpr}]t}}{\nu p^2+\eta(k^2+r^2)+\mu_{kpr}}\right|_{\eta=0} \sim \frac{1}{\nu p^2}, \qquad (t\to\infty). \tag{16}$$

Also as Fig.5(a), 6(a) show, we can use the relations $x \sim y \sim 0$, $z \sim 1$, and $r = k-p$. Then,

$$-\int^k dp \frac{1}{\nu p^2}\frac{p^2}{r}(1-x^2)\,(k-p)^m E_M(k) \sim -\frac{1}{\nu}k^m E_M(k). \tag{17}$$

(ii) Small p (large r, i.e., $k \sim r \gg p$, $x \sim z \sim 0$, $y \sim 1$)
In this case only the triad relaxation time μ_{kpr} is left. We assume that it is independent of time, so we can write μ_{kpr} like

$$\Theta^{\eta\eta\nu}_{krp}(k,t) \sim \frac{1}{\nu p^2+\mu_{kpr}} \sim \frac{1}{\mu_{kpr}}. \tag{18}$$

Then,

$$\sim -\int^k dr \frac{1}{\mu_{kpr}}(k^2 r^{m-1} - 2kr^m + r^{m+1})x(1-x^2)E_M(k) \sim 0. \tag{19}$$

The results, Eq.(17), (19) represent the first term in 'D' in Eq.(21). The other terms can be found in a similar way.

Then, the coupled equations of $E_V(k)$ and $E_M(k)$ are

$$\frac{\partial E_V(k)}{\partial t} = -\underbrace{\left(a_1 k^v + 2\nu k^2\right)}_{A} E_V(k) + \underbrace{\left(b_1 k^m - b_2 k^v\right)}_{B} E_M(k), \tag{20}$$

$$\frac{\partial E_M(k)}{\partial t} = \underbrace{\left(c_1 k^m + c_2 k^{m+2}\right)}_{C} E_V(k) - \underbrace{\left(d_1 k^m + d_2 k^{v+2}\right)}_{D} E_M(k). \tag{21}$$

The coefficients 'a_i', 'b_i', 'c_i', and 'd_i' are independent of 'k', and assumed to be independent of time for simplicity. The matrix form of these simultaneous differential equations is simply

$$\left[\begin{array}{c} E_V'(k) \\ E_M'(k) \end{array}\right] = \underbrace{\left[\begin{array}{cc} -A & B \\ C & -D \end{array}\right]}_{\mathcal{M}} \left[\begin{array}{c} E_V(k) \\ E_M(k) \end{array}\right]. \tag{22}$$

Eq.(22) can be solved diagonalizing the matrix '$\mathcal{M}$'. For this, the bases $E_V(k)$ and $E_M(k)$ need to be transformed using a transition matrix '$\mathcal{P}$' which is composed of eigenvectors of '$\mathcal{M}$':

$$\left[\begin{array}{c} E_V(k) \\ E_M(k) \end{array}\right] = \mathcal{P} \left[\begin{array}{c} V(k) \\ M(k) \end{array}\right], \quad \mathcal{P} = \left[\begin{array}{cc} B & B \\ A+\lambda_1 & A+\lambda_2 \end{array}\right]. \tag{23}$$

Then,

$$\begin{aligned} \left[\begin{array}{c} V'(k) \\ M'(k) \end{array}\right] &= P^{-1}\mathcal{M}P \left[\begin{array}{c} V(k) \\ M(k) \end{array}\right] = \left[\begin{array}{cc} \lambda_1 & 0 \\ 0 & \lambda_2 \end{array}\right] \left[\begin{array}{c} V(k) \\ M(k) \end{array}\right] \\ \Rightarrow \left[\begin{array}{c} V(k) \\ M(k) \end{array}\right] &= \left[\begin{array}{c} V_0(k)e^{\lambda_1 t} \\ M_0(k)e^{\lambda_2 t} \end{array}\right]. \end{aligned} \tag{24}$$

λ_1 and λ_2 are eigenvalues:

$$\lambda_1 = \frac{-(A+D) + \sqrt{(A+D)^2 - 4AD + 4BC}}{2}, \tag{25}$$

$$\lambda_2 = \frac{-(A+D) - \sqrt{(A+D)^2 - 4AD + 4BC}}{2}. \tag{26}$$

We choose a leading term in each elements with the consideration of their coefficients $k \sim p$ or $k \sim r$. Then the coefficients are like

$$A \sim 2\nu k^2, \quad B \sim b_1 k^m, \quad C \sim c_2 k^{m+2}, \quad D \sim d_2 k^{v+2}. \tag{27}$$

Here[4], since $AD - BC \sim k^{v+4} - k^{2m+2} \sim 0$ as $k \to \infty$, the eigenvalues converge to $\lambda_1 \sim 0, \quad \lambda_2 \sim -2\nu k^2$ as 'k' increases.

$E_V(k)$ and $E_M(k)$ are expressed like

$$\begin{bmatrix} E_V(k) \\ E_M(k) \end{bmatrix} = \begin{bmatrix} b_1 k^m & b_1 k^m \\ 2\nu k^2 & 0 \end{bmatrix} \begin{bmatrix} V_0(k) e^{\sim 0 \cdot t} \\ M_0(k) e^{-2\nu k^2 t} \end{bmatrix}. \tag{28}$$

If 'V_0' and 'M_0' are replaced by $E_{V0}(k) \sim k^v$ and $E_{M0}(k) \sim k^m$, we find the saturated solutions:

$$E_M(k) = 2\nu k^2 V_0(k) \sim 2\nu k^2 \frac{E_{M0}(k)}{2\nu k^2} \sim k^m, \tag{29}$$

$$E_V(k) = b_1 k^m \frac{E_{M0}(k)}{2\nu k^2} + b_1 k^m \left[- \frac{E_{M0}(k)}{2\nu k^2} + \frac{E_{V0}(k)}{b_1 k^m} \right] e^{-2\nu k^2 t} \sim k^{2m-2}. \tag{30}$$

For complete energy spectra, 'm' is required. But it is difficult to pinpoint a representative magnetic power spectrum because $E_M(k)$ is a continuously changing curve. Schekochihin et al. (2004) found '$m = 0$', peak of $E_M(k)$, but we do not think a peak can be a representative power spectrum that drops continuously with the wavenumber 'k'. On the other hand, Lazarian et al. (2004) found '$m = -1$' using a simulation with a strong background magnetic field $\mathbf{b}_{ext}$, a filling factor, and balance relation $\mathbf{B} \cdot \nabla \mathbf{B} \sim \nu \nabla^2 \mathbf{v}$. So we infer the index '$m = -1/2$' for the magnetic scaling factor in a system under the influence of a weak background magnetic field. Then, from Eq.(30) we get $E_V(k)$ 'k^{-3}', which matches the simulation results well. Also this makes '$AD - BC \sim 0$', i.e., '$\lambda_1 \sim 0$' and '$\lambda_2 < 0$' so that the energy spectra become independent of time when they are saturated. If '$m = -1$' is chosen, '$E_V(k) \sim k^{-4}$' and $E_M(k) \sim k^{-1}$', coincident with the results of (Cho et al. 2003; Lazarian et al. 2004). A simple relation $E_M^2/E_V = k^2$ can be derived in high Pr_M.

4. Discussion

The analytic and simulation job in this paper are to realize the high Pr_M plasma state in ICM. Magnetic field affects the fluid motion through Lorentz force $q\mathbf{v} \times \mathbf{B}$ to cause the rotational motion of ionized particles around the magnetic field. The effect of magnetic field, leading to the anisotropic system, competes with that of collision which transfers momentum to make the system isotropic. In fact the weakly collisional ICM plasma has few proper

[4]The dimensional analysis of Eq.(20) implies $2m \sim v + 2$ when the system is saturated.

ways to constrict the anisotropic tendency. However, if background magnetic field is not too strong, a system driven by a random isotropic force in large scales eventually becomes isotropic overall although small scale eddies still tend to be anisotropic under the influence of magnetic field.

Simulation of high Pr_M tells us some important features. The viscous scale k_ν is extended toward the much smaller diffusivity scale k_η, and nontrivial E_V in this extended scale is a prerequisite to the growth of E_M. For the local and nonlocal energy transfer, besides energy gap in kinetic and magnetic eddies, additional specific geometrical relation between $\mathbf{v}$ and $\mathbf{B}$ is required. For example smaller $E_M(k)$ than $E_V(k)$ in larger scales boosts the nonlocal kinetic energy transfer from kinetic to magnetic eddies; and, smaller $E_V(k)$ than $E_M(k)$ in small scale helps the energy transfer from magnetic to kinetic eddies. However, the energy transfer in magnetic eddies is possible only when $\mathbf{B}\cdot\nabla\mathbf{V}$ (nonlocal transfer) or $-\mathbf{V}\cdot\nabla\mathbf{B}$ (local transfer) is nontrivial. As a result of all these effects with the viscous damping, $E_V \sim k^{-3}$ and smoothly changing E_M are finally saturated in the subviscous regime. Analytic analysis shows the viscous effect $\sim \nu k^2$ coupled with E_M^2 induces this unusual spectrum. (Eq.29, 30).

Finally, as mentioned the anisotropic features of small scale cannot affect the large scale driven by the isotropic force. However, if there is an instability due to the anisotropic pressure in microscale, plasma distribution in the whole system may change. We have not discussed the influence of microscale instability due to the anisotropic pressure including viscosity and conductivity on the MHD system in this paper, but we will leave these important topics for the future research on ICM.

5. Acknowledgements

KP acknowledges support from the National Research Foundation of Korea through grant 2007-0093860. DP acknowledges the Korea Ministry of Education, Science and Technology, Gyeongsangbuk-Do and Pohang City for the support of the Junior Research Group at APCTP

A. Appendix

For '$A1$' in Eq.(11), we differentiate this triple correlation term over time to use Eq.(8), (9). Then, we have

$$\begin{aligned}
&\big[\frac{\partial}{\partial t}+\nu\big(k^2+p^2+r^2\big)\big]\big\langle v_q(p)v_m(r)v_i(-k)\big\rangle_{A1}= \\
&\big\langle\big[\big(\frac{\partial}{\partial t}+\nu k^2\big)v_i(-k)\big]v_q(p)v_m(r)\big\rangle+\big\langle v_i(-k)\big[\big(\frac{\partial}{\partial t}+\nu p^2\big)v_q(p)\big]v_m(r)\big\rangle \\
&+\big\langle v_i(-k)v_q(p)\big[\big(\frac{\partial}{\partial t}+\nu r^2\big)v_m(r)\big]\big\rangle=\langle vvvv\rangle+\langle vvBB\rangle... \qquad \text{(A1)}
\end{aligned}$$

If we see the first term, for example,

$$\begin{aligned}
\big\langle\big[\big(\frac{\partial}{\partial t}+\nu k^2\big)v_i(-k)\big]v_j(p)v_m(r)\big\rangle\delta_{p+r,k}=\sum_{j,l}\big[&M_{ins}(-k)\langle v_n(j)v_s(l)v_q(p)v_m(r)\rangle \\
&-M_{ins}(-k)\langle B_n(j)B_s(l)v_q(p)v_m(r)\rangle\big]\delta_{j+l,-k}. \qquad \text{(A2)}
\end{aligned}$$

the differentiation generates the fourth order correlation. Another differentiation just induces the fifth order correlation. So we need an assumption to close this equation. It is known that statistically turbulent quantities follow a normal distribution. And the fourth-order term $\langle uuuu\rangle$ can be decomposed into the combination of second-order correlation terms like below: quasi-normal approximation (Proudman et al. 1954; Tatsumi 1957):

$$\langle u_1u_2u_3u_4\rangle=\langle u_1u_2\rangle\langle u_3u_4\rangle+\langle u_1u_3\rangle\langle u_2u_4\rangle+\langle u_1u_4\rangle\langle u_2u_3\rangle. \qquad \text{(A3)}$$

So if these second order correlation terms are replaced by energy spectrum expressions as follows:

$$\begin{aligned}
4\pi k^2\langle v_i(k)v_q(k')\rangle &= P_{iq}(k)E_V(k)\delta_{k+k',0}, \qquad \text{(A4)}\\
4\pi k^2\langle B_i(k)B_q(k')\rangle &= P_{iq}(k)E_M(k)\delta_{k+k',0}, \\
4\pi k^2\langle B_i(k)v_q(k')\rangle &= P_{iq}(k)H_{BV}(k)\delta_{k+k',0}. \\
(P_{iq}=\delta_{iq}-\frac{k_ik_q}{k^2}) &
\end{aligned}$$

Eq.(A1) can be rewritten like

$$\begin{aligned}
&\big[\frac{\partial}{\partial t}+\nu\big(k^2+p^2+r^2\big)\big]\big\langle v_q(p)v_m(r)v_i(-k)\big\rangle_{A1}= \\
&2M_{ins}(-k)\sum_{p,r}(4\pi p^2)^{-1}(4\pi r^2)^{-1}P_{nq}(p)P_{ms}(r)[E_V(p)E_V(r)-H_{BV}(p)H_{BV}(r)]+ \\
&2M_{qns}(p)\sum_{p,r}(4\pi k^2)^{-1}(4\pi r^2)^{-1}P_{in}(k)P_{ms}(r)[E_V(k)E_V(r)-H_{BV}(k)H_{BV}(r)]+ \\
&2M_{mns}(r)\sum_{p,r}(4\pi k^2)^{-1}(4\pi r^2)^{-1}P_{in}(k)P_{js}(p)[E_V(k)E_V(p)-H_{BV}(k)H_{BV}(p)] \\
&\equiv L^{vv1}_{iqm}(k,p,r;t). \qquad \text{(A5)}
\end{aligned}$$

However, when the fourth-order correlation is decomposed into the combinations of second order terms, the summation of decomposed ones, i.e., right hand side of Eq.(A3), can be larger than its actual value. This can cause a negative energy spectrum, which cannot be allowed (Ogura 1963). So (Orszag 1970) introduced an eddy damping coefficient μ_{kpr} of which dimension is '$\sim 1/t$'. Its more detailed expression (Pouquet et al. 1976) can be contrived, but the dimension '$\sim 1/t$' does not change. We assume it to be sort of a reciprocal of time constant for simplicity in this paper. Then, with a simple integration we can find the third correlation term:

$$\big\langle v_q(p)v_m(r)v_i(-k)\big\rangle_{A1}=\int^t e^{-(\nu(k^2+p^2+r^2)+\mu_{kpr})(t-\tau)}L^{vv1}_{iqm}(k,p,r;\tau)d\tau. \qquad \text{(A6)}$$

We can also calculate the representation of '$A3$' in the same way:

$$\big\langle B_q(p)B_m(r)v_i(-k)\big\rangle_{A3}=\int^t e^{-(\nu k^2+\mu_{kpr})(t-\tau)}L^{vv3}_{iqm}(k,p,r;\tau)d\tau. \qquad \text{(A7)}$$

Since '$A2$' and '$A4$' are '-$A1$' and '-$A3$' respectively, Eq.(11) are

$$\begin{aligned}
\big(\frac{\partial}{\partial t}+2\nu k^2\big)\langle v_i(k)v_i(-k)\rangle=\sum_{p+r=k}2M_{iqm}(k)\Big[&\int^t e^{-(\nu(k^2+p^2+r^2)+\mu_{kpr})(t-\tau)}L^{vv1}_{iqm}(k,p,r;\tau)d\tau \\
&-\int^t e^{-(\nu k^2+\mu_{kpr})(t-\tau)}L^{vv3}_{iqm}(k,p,r;\tau)d\tau\Big]. \qquad \text{(A8)}
\end{aligned}$$

If $L^{vv1}_{iqm}(k,p,r;\tau)$ or $L^{vv3}_{iqm}(k,p,r;\tau)$ is larger than $(\nu(k^2+p^2+r^2)+\mu_{kpr})^{-1}$ or $(\nu k^2+\mu_{kpr})^{-1}$, this equation can be markovianized. Thus, with the definition of a triad relaxation time $\Theta(t)$

(Frisch et al. 1975) we get

$$\begin{aligned}
&\Big(\frac{\partial}{\partial t}+2\nu k^2\Big)E_V(k)= \\
&\sum_{p+r=k} 4\pi k^2 M_{iqm}(k)\Bigg[\left(\frac{1-e^{-(\nu(k^2+p^2+r^2)+\mu_{kpr})t}}{\nu(k^2+p^2+r^2)+\mu_{kpr}}\right)L^{vv1}_{iqm}(k,p,r;t) \\
&-\left(\frac{1-e^{-(\nu k^2+\mu_{kpr})t}}{\nu k^2+\mu_{kpr}}\right)L^{vv3}_{iqm}(k,p,r;t)\Bigg] \\
&\equiv \sum_{p+r=k} 4\pi k^2 M_{iqm}(k)\Bigg[\Theta^{\nu\nu\nu}_{kpr}(t)L^{vv1}_{iqm}(k,p,r;t)-\Theta^{\nu\eta\eta}_{kpr}(t)L^{vv3}_{iqm}(k,p,r;t)\Bigg].
\end{aligned} \tag{A9}$$

Using a trigonometric relation: $\mathbf{k}\cdot\mathbf{p}=kpz$, $\mathbf{k}\cdot\mathbf{r}=kry$, $\mathbf{p}\cdot\mathbf{r}=-prx$ (Fig.5(a)) and $d\mathbf{p}\,d\mathbf{r}=\frac{2\pi pr}{k}dp\,dr$, we can simplify this expression:

$$\frac{1}{2}\int dp\,dr\,\Theta^{\nu\nu\nu}_{kpr}(t)\frac{k^3}{p\,r}(1-2y^2z^2-xyz)[E_V(p)E_V(r)-H_{BV}(p)H_{BV}(r)]. \tag{A10}$$

Eq.(13), (14) can be derived using a similar way.

REFERENCES

Batchelor, G. K. 1950, Proc. Roy. Soc. London, Ser. A, 201, 405

Bovino, S., Schleicher, D., R., G., & Schober, J., 2013, New J. Phys., 15, 013055

Brandenburg, A. 2001, ApJ, 550, 824

Chew, G., F., Goldberger, M., L., & Low, F., E., 1956, RSPSA, 236, 112

Cho, J., Lazarian, A., & Vishniac, E., 2003, ApJ, 595, 812

Cho, J., Vishniac, E., Beresnyak, A., Lazarian, A., & Ryu, D., 2009, ApJ, 693, 1449

Cho, J., & Yoo, H., 2014, ApJ, 780, 99

Cho, J., 2014, 797, 133

Frisch, U. , Pouquet, A., Leorat, J. & Mazure, A., 1975, J. Fluid Mech., 68, 769

Jones, T. W., 2008, Astronomical Society of the Pacific Conference Series, 386, 398

Kazantsev, A., P., 1968, JETP, 26, 1031

Kleeorin, N., Mond, M., & Rogachevskii, I., 1996, A&A, 307, 293

Kolmogorov, A., 1941, Akademiia Nauk SSSR Doklady, 30, 301

Kraichnan R. H. & Nagarajan, S., 1967, Physics of Fluids, 10, 859

Krause, F. & Rädler, K. H., 1980, Mean-field magnetohydrodynamics and dynamo theory

Kulsrud, R. M. & Anderson, S. W. 1992, ApJ, 396, 606

Lazarian, A., Vishniac, E. T., & Cho, J., ApJ, 2004, 603, 180

Leslie, D. C. & Leith, C. E., 1975, Physics Today, 28, 59

McComb, W. D., 1990, The physics of fluid turbulence

Moffatt, H. K., 1978, Magnetic Field Generation in Electrically Conducting Fluids

Narayan, R., & Medvedev, M. V., 2001, ApJ, 562, L129

Ogura, Y., 1963, J. Fluid Mech., 16, 33

Orszag, S. A., 1970, J. Fluid Mech., 41, 363

Park, K., 2013, MNRAS, 434, 2020

Park, K., & Blackman, E. G., 2012a, MNRAS, 419, 913

Park, K., & Blackman, E. G., 2012b, MNRAS, 423, 2120

Pouquet, A., Frisch, U., & Leorat, J., 1976, J. Fluid Mech., 77, 321

Proudman, I., & Reid, W. H., 1954, Royal Society of London Philosophical Transactions Series A, 247, 163

Ruzmaikin, A. A., & Shukurov, A. M., 1982, Astrophysics and Space Science, 82, 397

Ryu, D., Kang, H., Cho, J., & Das, S., 2008, SCIENCE, 320, 909

Ryu, D., Porter, D. H., Cho, J., & Jones, T., W., 2012, AAS...21933803R

Santos-Lima, R., de Gouveia Dal Pino, E., M., Falceta-Gonçalves, D., Lazarian, A., & Kowal, G., 2011, IAUS, 274, 482

Santos-Lima, R., de Gouveia Dal Pino, E., M., Kowal, G., Falceta-Gonçalves, D., Lazarian, A., & Nakwacki, M., S., 2014, ApJ, 781, 84

Schekochihin, A. A., Maron, J. L., Cowley, S. C., & McWilliams, J. C., 2002, ApJ, 576, 806

Schekochihin, A. A., Cowley, S. C., Taylor, S. F., Maron, J. L., & McWilliams, J. C., 2004, ApJ, 612, 276

Schekochihin, A. A., Cowley, S. C., Kulsrud, R. M., Hammett, G. W., & Sharma, P., 2005, ApJ, 629, 139

Schekochihin, A. A., Cowley, S. C., Kulsrud, R. M., Hammett, G. W., & Sharma, P., 2005, ApJ, 629, 139

Schekochihin, A. A., Cowley, S. C., Kulsrud, R. M., Rosin, M. S., & Heinemann, T., 2008, Physical Review Letters, 100(8), 081301

Schekochihin, A. A., Cowley, S. C., Rincon, F., $ Rosin, M. S., 2010, MNRAS, 405, 291

Schober, J., Schleicher, D., Federrath, C., Klessen, R., & Banerjee, R., 2012, Phys. Rev. E., 85, 026303

Tatsumi, T., 1957, Royal Society of London Proceedings Series A, 239, 16

Vogt, C., & Enßlin, T., A., 2003, A&A, 412, 373

Yoshizawa, A., 2011, Hydrodynamic and Magnetohydrodynamic Turbulent Flows: Modelling and Statistical Theory (Fluid Mechanics and Its Applications

Yousef, T., A., Rincon, F., & Schekochihin, A., A., 2007, JFM, 575, 111

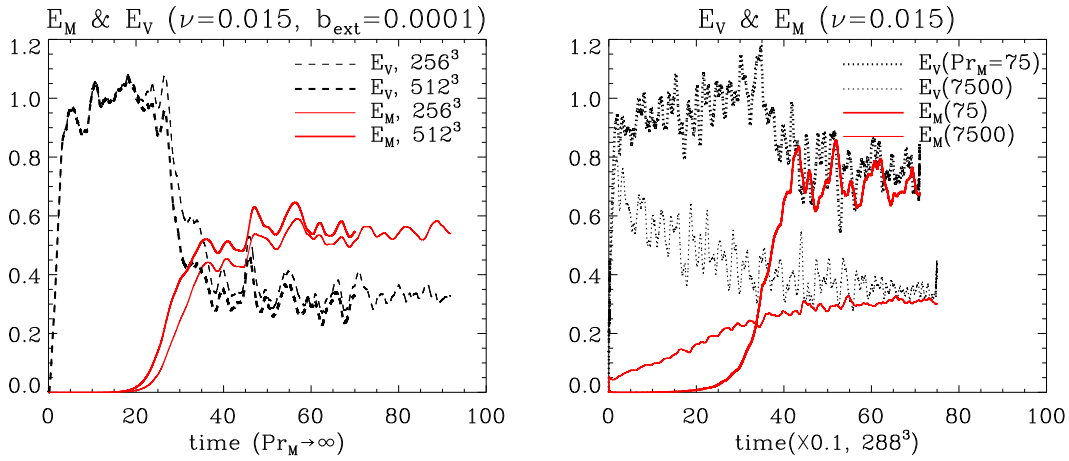

(a) (b)

Fig. 1.— (a) Normalized $E_V(t)$ and $E_M(t)$ for the incompressible fluid ($Pr_M \to \infty$, resolution 256^3 and 512^3). (b) Normalized $E_V(t)$ and $E_M(t)$ for the compressible fluid ($Pr_M = 75$ and $Pr_M = 7500$, resolution 288^3). Time scale is contracted by 10% ($\times 0.1$).

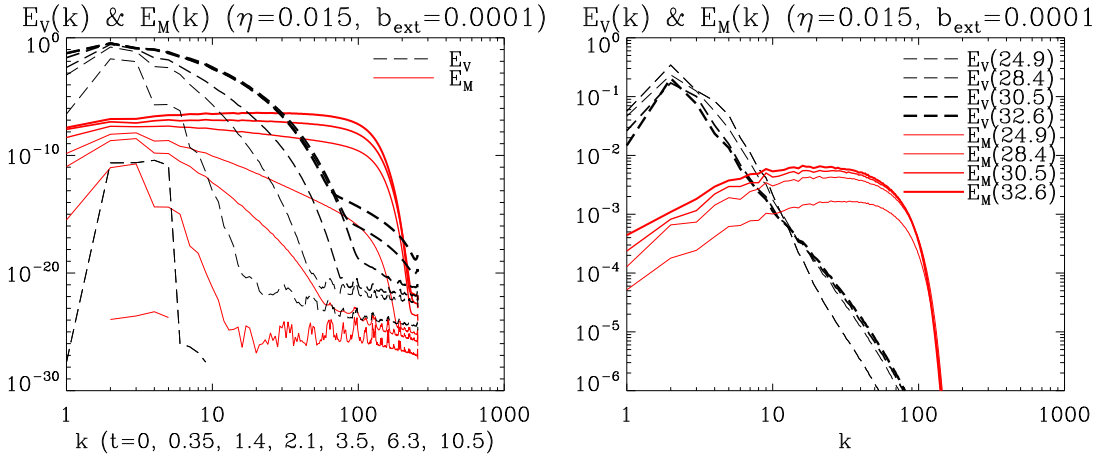

(a) (b)

Fig. 2.— Energy spectra of incompressible fluid ($Pr_M \to \infty$) (a) $E_V(k)$ and $E_M(k)$ in the early time regime ($t \leq 10.5$) (b) $E_V(k)$ and $E_M(k)$ in $24.9 \leq t \leq 32.6$. As E_M grows, large scale kinetic energy is transferred to magnetic eddies, but kinetic eddies in subviscous scale receive energy from the magnetic eddies.

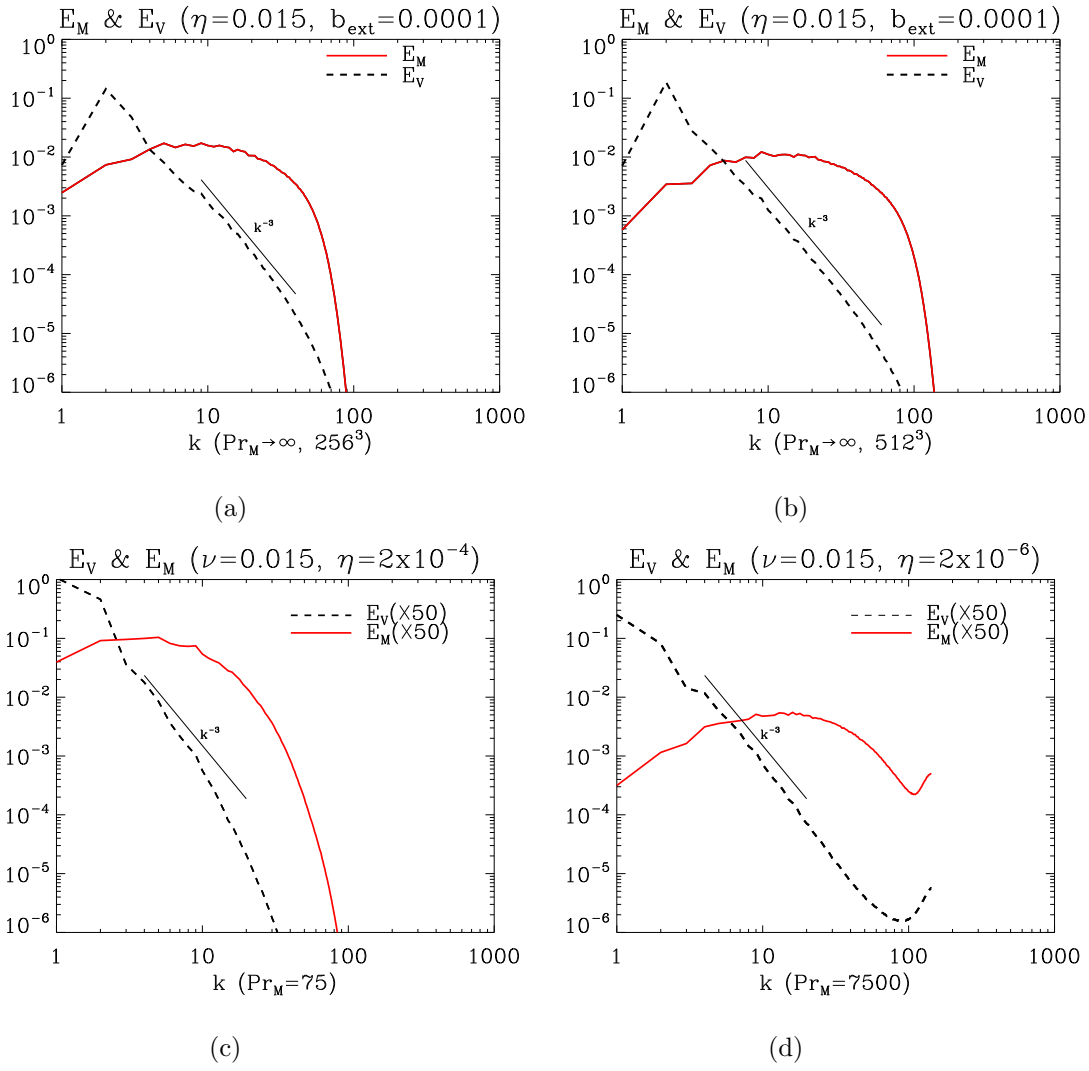

Fig. 3.— (a), (b) Saturated $E_V(k)$ and $E_M(k)$ with resolution 256^3 and 512^3 for the incompressible fluid. (c), (d) Saturated $E_V(k)$ and $E_M(k)$ for the compressible fluids with resolution 288^3. Saturated energy level of $Pr_M = 75$ is higher than that of $Pr_M = 7500$. Bottle neck effect appears.

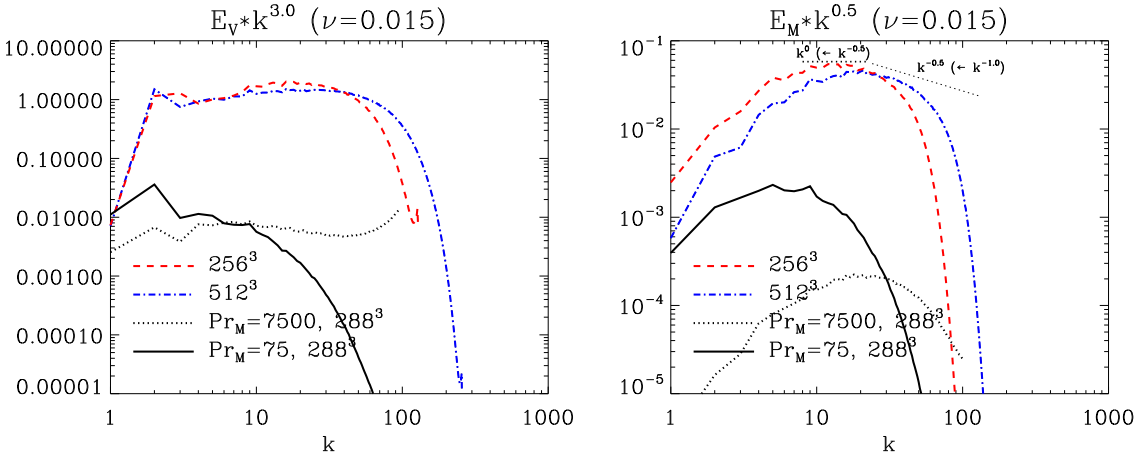

(a) (b)

Fig. 4.— (a) Compensated energy spectrum $k^3 E_V(k)$. (b) $k^{0.5} E_M(k)$. The flat reference line k^0 means $k^{-1/2}$ in $E_M(k)$, and slanted line $k^{-0.5}$ is the scaling invariant line k^{-1}.

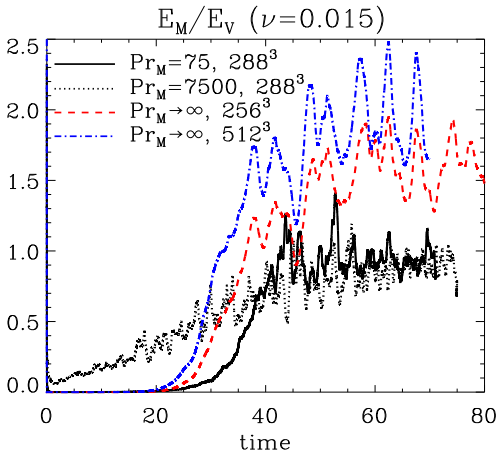

(a)

Fig. 5.— The ratio E_M/E_V of hyper diffusivity increases with resolution. In case of physical diffusivity the equipartition of E_M and E_V appears.

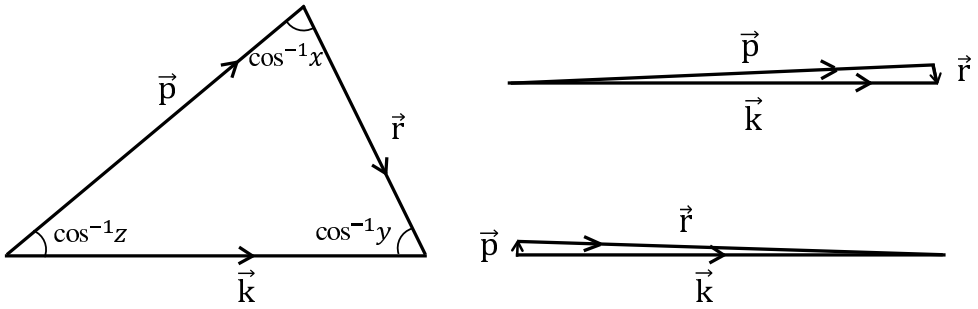

(a) $\mathbf{p}+\mathbf{r}+\mathbf{k}$ (b) $k \sim p \gg r$, $k \sim r \gg p$

Fig. 6.— (a) The summation of three wave numbers should satisfy the condition $\mathbf{p}+\mathbf{r}+\mathbf{k}=0$ (b) Upper triangle is the case of large $\mathbf{p}$ (small $\mathbf{r}$): $k \sim p \gg r$, $x \sim y$, $z \sim 1$, and lower one is for large $\mathbf{r}$ (small $\mathbf{p}$): $k \sim r \gg p$, $x \sim z$, $y \sim 1$.